RSC Advances




ROYAL SOCIETY OF CHEMISTRY

www.rsc.org/advances

Journal Name

Paper

# Fabrication of $Ag/Fe_2O_3/ZnO$ Ternary Composite with Enhanced Photocatalytic Performance

Received 00th January 20xx,
Accepted 00th January 20xx

DOI: 10.1039/x0xx00000x

www.rsc.org/

Jia-gen Wu‡, Ting Fang‡, Ran Cai, Shao-yang Li, Yue Wang, Cui-e Zhao and Ang Wei *

A novel $Ag/Fe_2O_3/ZnO$ ternary composite was fabricated by chemical deposition and photochemical deposition methods. The structure and optical properties were characterized by X-ray diffraction (XRD), scanning electron microscopy (SEM), transmission electron microscopy (TEM) and ultraviolet-visible spectrophotometer. The $Ag/Fe_2O_3/ZnO$ ternary composite exhibited a greater improvement in photocatalytic activity compared with $Fe_2O_3/ZnO$ or Ag/ZnO binary composite. The degradation rate of $Ag/Fe_2O_3/ZnO$ towards methyl orange (MO) and iodoform ($CHI_3$) within 120 min was 80% and 94%, respectively. More importantly, the $Ag/Fe_2O_3/ZnO$ had much higher degradation efficiency towards iodoform, indicating the efficient and selective degradation characteristics. The results show that the $Ag/Fe_2O_3/ZnO$ ternary composite holds great potential in removing of carcinogenic iodoform from sewage.

## 1. Introduction

Environment and human health are now threatened by a lot of pollutants in wastewater. The harm is still so great despite of the presence of low amount of halogenated hydrocarbon in wastewater, for example, iodoform that can even cause cancer [1-3]. Thus the removal of such toxic organic pollutants in wastewater is a highly essential issue. Semiconductor photocatalysts such as $TiO_2$ and ZnO can be a green and efficient technology in the field of sewage treatment, because they can effectively dispose many organic pollutants in the sewage compared with other approaches. Additionally, most photocatalytic materials are non-toxic, stable and low-cost [4, 5].

Although ZnO have a lot of advantages such as high quantum efficiency, non-toxic and strong ultraviolet absorption [6], its catalytic efficiency is still unideal. The main reasons include: (1) The band gap of ZnO is too wide, only the ultraviolet part of the sun light can be used; (2) ZnO is amphoteric oxide semiconductor, it easily dissolved in strong acid and alkali solution; (3) The electron-hole pairs in ZnO are easy to recombine, which reduces the photocatalytic efficiency. In this regard, combining ZnO with other metal compounds such as CuO and $Fe_2O_3$ has been proved to be effective in improving the photocatalytic performance of ZnO. However, ZnO binary composite materials also have some defects. It cannot selectively photodegrade some hazard pollutants in wastewater, especially halogenated hydrocarbons. Furthermore, the degradation efficiency decreases obviously when there is a variety of pollutants in wastewater. Recent studies have found that ZnO-based ternary composites have great superiority than binary composites [7, 8]. Besides, they have the function of selective degradation of some pollutants [9]. Also, it has been found that Ag has a strong adsorption of high carcinogenic halogenated hydrocarbon [10].

In this work, the $Ag/Fe_2O_3/ZnO$ ternary composite was synthesized by chemical deposition and photochemical deposition process. The photocatalytic activity of $Ag/Fe_2O_3/ZnO$ was investigated in comparison with $Fe_2O_3/ZnO$ or Ag/ZnO. Furthermore, the effects of structure and interfacial electronic interactions among ZnO, $Fe_2O_3$ and Ag on the photocatalytic activity were also investigated. The $Ag/Fe_2O_3/ZnO$ ternary composite had effective photodegradation toward MO and iodoform under irradiation of simulated daylight, and it had higher degradation efficiency towards iodoform. The results indicated the potential applications of $Ag/Fe_2O_3/ZnO$ in sewage treatment.

## 2. Experiments

### 2.1 Preparation of the $Ag/Fe_2O_3/ZnO$ ternary composite

Firstly, ZnO seed layer was prepared by a sol-gel method. Briefly, 40 ml anhydrous ethanol, 0.5 M zinc acetate-2-hydrate, and 0.5 M ethanol amine were mixed, and stirred at 70 ℃ for 3 h. The resultant sol was transparent. The solution was then spin-coated on the glass substrate at 500 rpm for 10 s and

*Key Laboratory for Organic Electronics and Information Displays & Institute of Advanced Materials (IAM), Jiangsu National Synergetic Innovation Center for Advanced Materials (SICAM), Nanjing University of Posts & Telecommunications, 9 Wenyuan Road, Nanjing 210023, China.*
*Correspondence author. Email: wei1177@126.com

‡ These authors contributed equally to this work.

3000 rpm for 30 s, respectively. After that, the glass substrate was heated at 300°C for 2h to remove the solvent. Subsequently, the growth of ZnO nanorod (NR) was carried out by suspending the glass substrate in a 40 mL beaker that filled with an equimolar aqueous solution of 0.1 M zinc nitrate hexahydrate ($Zn(NO_3)_2{\cdot}6H_2O$), and 0.1 M methenamine ($C_6H_{12}N_4$, HMT) at 75 °C for 3 h [11, 12].

$Fe_2O_3$ nanoparticles were then deposited on the ZnO nanorod by photochemical deposition. The ZnO nanorods-coated substrate was immersed in a mixture of 4 mM $FeCl_3{\cdot}6H_2O$ and $NaNO_3{\cdot}6H_2O$ aqueous solution, and then irradiated with UV light for 1 h (wavelength 365 nm, power 56 W, working distance 0.3 m) [13, 14].

Ag nanoparticles were further prepared by photochemical deposition. $Fe_2O_3$/ZnO nanorods-coated substrate was immersed in a 1 mM $AgNO_3$ and $NaNO_3{\cdot}6H_2O$ aqueous solution, and then irradiated with UV light (wavelength 365 nm, power 56 W, working distance 0.3 m) at room temperature for 40 min. The prepared sample was post-annealed in ambient air at 400 ℃ for 2 h to obtain the crystal structure.

### 2.2 Characterization

The crystal structure of the products was characterized by X-ray diffraction (XRD , Siemens D5005). The scanning electron microscopy (SEM, S4800) was employed to investigate the morphology. Transmission electron microscopy (TEM), high-resolution electron microscopy (HRTEM) and selected area electron diffraction (SAED) were measured with a Tecnai G2 F20 S-TWIN. The UV–vis absorption spectra were analyzed by UV-2401PC spectrometer.

### 2.3 Photocatalytic studies

Iodoform（halogenated hydrocarbon）and MO (organic dye) are two common pollutants in wastewater. Iodoform and MO were chosen to investigate the photo-degratation characteristic of Ag/$Fe_2O_3$/ZnO ternary composite, $Fe_2O_3$/ZnO and Ag/ZnO binary composite. Samples were put in 30 ml of iodoform solution (1.65 mmg/L) and MO solution (6.67 mmg/L) with irradiation of simulated sunlight (xenon lamp, wavelength 320-780 mm, the light intensity at the sample is about 50 mW/cm$^2$), respectively. The solutions of iodoform and MO were taken every 30 min to analyze their ultraviolet absorbance, respectively.

To investigate the reusability of Ag/$Fe_2O_3$/ZnO ternary composite, the Ag/$Fe_2O_3$/ZnO modified glass substrates were put into 30 ml of iodoform solution (1.65 mmg/L) and MO solution (6.67 mmg/L) under irradiation of simulated sunlight for 5 cycles, respectively. Each cycle, the iodoform and MO solutions were degraded by Ag/$Fe_2O_3$/ZnO for 120 min and measured their maximum absorbance, respectively. In the next cycle, replacing the solutions of iodoform and MO, the same Ag/$Fe_2O_3$/ZnO modified glass substrates were used again to degrade iodoform and MO for 120 min and measured their maximum absorbance, respectively.

## 3. Result and Discussion

### 3.1 Characterization of materials

Fig. 1 shows the XRD pattern of the as-prepared sample. The typical diffraction peaks (0 0 2), (1 0 2), (1 1 0), (1 0 3), (2 0 1) of hexagonal wurtzite ZnO are observed, which are in good agreement with standard patterns (JSPDSNO.36-1451). In addition, three diffraction peaks (2 0 6), (2 1 12), (5 2 1) (JCPDSNO.13-0458) of $Fe_2O_3$ and four diffraction peaks (2 2 0), (3 1 1), (3 3 1), (4 2 0) (JSPDSNO.01-1164) of Ag are observed, revealing that the obtained Ag/$Fe_2O_3$/ZnO ternary composite has good crystalline structure.

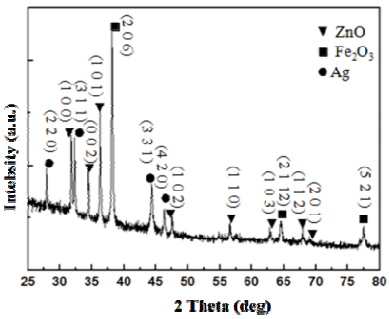


**Fig. 1** The XRD patterns of the Ag/$Fe_2O_3$/ZnO ternary composite.

The as-prepared samples are characterized by SEM. As shown in Fig. 2a, it is obvious that the wurtzite ZnO rods are hexagonal structure, and the surface is relatively smooth (Fig. 2a inset). Under the irradiation with UV light, the $Fe_2O_3$ nanoparticles are coated on the surface of ZnO to form $Fe_2O_3$/ZnO binary composite (Fig. 2b), resulting in a rough layer on the nanorods (Fig. 2b inset). After the decoration of Ag nanoparticles, the granular materials are observed on the surface of $Fe_2O_3$/ZnO (Fig. 2c and 2c inset), indicating the formation of the Ag/$Fe_2O_3$/ZnO ternary composite.

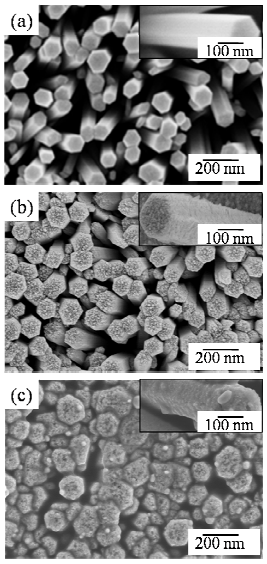

**Fig. 2** SEM images of (a) ZnO nanorod arrays, (b) $Fe_2O_3$/ZnO binary composite, and (c) Ag/$Fe_2O_3$/ZnO ternary composite.

To further clarify the structure and morphology of Ag/$Fe_2O_3$/ZnO ternary composite, HRTEM was performed. As shown in Fig. 3a, it is noted that the product is hierarchical structures. The high-magnification image of Fig. 3a (indicated by the white rectangle) suggests that the lattice spacing is about 0.248 nm, 0.155 nm and 0.144 nm (Fig. 3b), corresponding to the (1 0 1) plane of ZnO, the (5 2 1) plane of $Fe_2O_3$, and the (2 2 0) plane of Ag, respectively. The data indicates the existence of ZnO, $Fe_2O_3$ and Ag in the composite. The corresponding selected area electron diffraction (SAED) patterns further confirm the successful formation of Ag/$Fe_2O_3$/ZnO ternary composite (Fig. 3c).

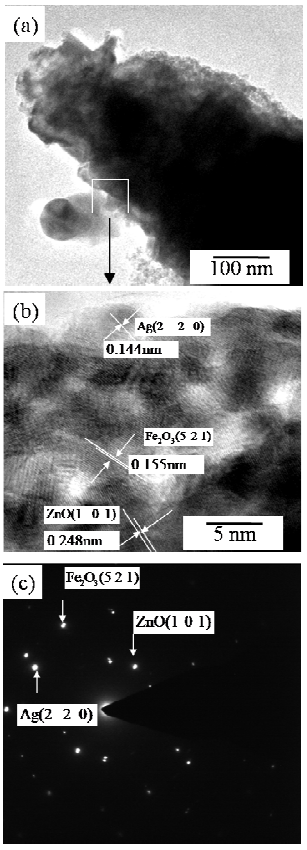


**Fig. 3** (a) TEM image of the Ag/$Fe_2O_3$/ZnO ternary composite, (b) HR-TEM image of the area indicated by white rectangle in (a), and (c) the SAED pattern of (a).

### 3.2 Growth mechanism

The proposed growth mechanism of Ag/$Fe_2O_3$/ZnO ternary composite is shown in Fig. 4. Firstly, with the addition of HMT and $Zn(OH)_4^{2-}$, the ZnO rod arrays were coated on the glass substrate with ZnO seed layer under hydrothermal treatment at 75 ℃ [15] (Fig. 4a). Secondly, under UV irradiation, ZnO could form electronic-hole pairs. As a result, a great deal of $OH^-$ and $Fe^{3+}$ were deposited on the surface of ZnO nanorod to form $[Fe(OH)_4]^-$ ions, and then they removed $OH^-$ and $H_2O$ to form $Fe_2O_3$ [16] (Fig. 4b). Likewise, with the continued UV irradiation, more and more $Fe_2O_3$ particles are obtained, leading to a thick layer covered on the surface of ZnO (Fig. 4c). Finally, in aqueous solution of $AgNO_3$ and $NaNO_3 \cdot 6H_2O$, $Ag^+$ and $OH^-$ were deposited on the surface of $Fe_2O_3$/ZnO, generating nanosized silver particles [17] (Fig. 4d).

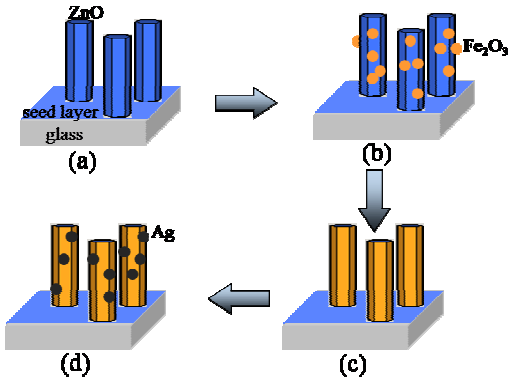


**Fig. 4** The proposed growth model of Ag/$Fe_2O_3$/ZnO ternary composite, (a) ZnO nanorods were grown on the substrate of glass, (b) $Fe_2O_3$ nanoparticles were attached to the surface of ZnO, (c) the $Fe_2O_3$ layer was coated on the surface of ZnO, and (d) Ag nanoparticles were uniformly deposited on the surface of $Fe_2O_3$/ZnO to form the Ag/$Fe_2O_3$/ZnO ternary composite.

### 3.3 Photocatalytic activity

Fig. 5 shows UV–vis absorption spectra of Ag/ZnO, $Fe_2O_3$/ZnO and Ag/$Fe_2O_3$/ZnO, respectively. Remarkably, the absorption wavelength of Ag/$Fe_2O_3$/ZnO ternary composite is up to 650 nm, which is much wider than that of Ag/ZnO or $Fe_2O_3$/ZnO. The result indicates that the Ag/$Fe_2O_3$/ZnO can improve the absorption intensity in the visible region. Therefore, the Ag/$Fe_2O_3$/ZnO ternary composite has great potential in terms of light degradation.

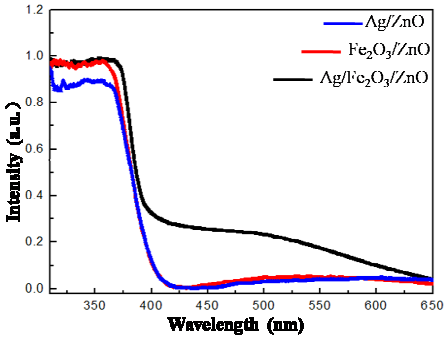


**Fig. 5** UV–vis absorption spectra of Ag/ ZnO, $Fe_2O_3$/ZnO and Ag/$Fe_2O_3$/ZnO.

The photodegrade efficiency of $Fe_2O_3$/ZnO, Ag/ZnO, and Ag/$Fe_2O_3$/ZnO under illumination and without illumination (Fig. S1) were investigated. To calculate the concentration of the iodoform and MO solutions, the solutions were collected every 30 min and measured the absorption intensity at their maximum absorbance wavelength, respectively. Fig. 6 shows UV-vis absorption spectra of iodoform and MO degraded by

$Fe_2O_3$/ZnO, Ag/ZnO, and Ag/$Fe_2O_3$/ZnO, respectively. When Ag/ZnO was used as the photocatalyst materials, the characteristic absorption peaks of iodoform and MO dropped to about 44% and 50% of their initial absorption intensity after 120 min (Fig. 6a), respectively. As for $Fe_2O_3$/ZnO, the absorption peaks of iodoform and MO reduced to about 40% of their initial absorption intensity after 120 min (Fig. 6b), respectively. Interestingly, when the Ag/$Fe_2O_3$/ZnO was used, the absorption peaks of iodoform and MO rapidly decreased to about 5% and 22% of their initial intensity after 120 min, respectively (Fig. 6c). Obviously, the Ag/$Fe_2O_3$/ZnO ternary composite had much higher degradation efficiency towards iodoform and MO compared to Ag/ZnO or $Fe_2O_3$/ZnO.

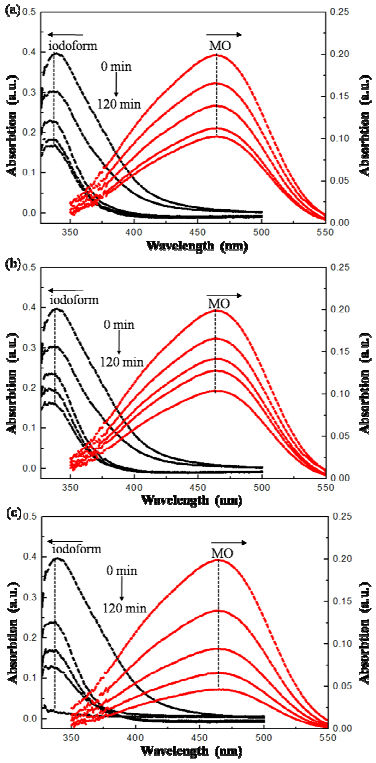


**Fig. 6** Time-dependent absorption spectra of iodoform and MO degraded by (a) Ag/ZnO, (b) $Fe_2O_3$/ZnO and (c) Ag/$Fe_2O_3$/ZnO.

By considering the peak intensity of MO and iodoform, we have plotted the corresponding degradation rates of $Fe_2O_3$/ZnO, Ag/ZnO and Ag/$Fe_2O_3$/ZnO, as shown in Fig. 7. Degradation efficiency (y-axis), is defined as $(1 - C/C_0) \times 100\%$, and the x-axis is reaction time in units of minute. $C_0$ is the initial concentration after the equilibrium adsorption, and C is the remaining concentration of iodoform and MO [18, 19]. Under irradiation of simulated sunlight, the degradation efficiency of Ag/$Fe_2O_3$/ZnO for iodoform and MO were 94% and 80% (curve 1 and 2) after 120 min respectively, much higher than them of $Fe_2O_3$/ZnO (58% and 60%, curve 3 and 4), or Ag/ZnO (56% and 50%, curve 5 and 6). In addition, in the mixture of three organics, the degradation efficiency of Ag/$Fe_2O_3$/ZnO for iodoform, MO and RhB was 89%, 45% and 40% (Fig. S2), respectively. The data indicated that the Ag/$Fe_2O_3$/ZnO exhibited a greater improvement in photocatalytic activity compared with $Fe_2O_3$/ZnO or Ag/ZnO. More importantly, the results also suggested that the Ag/$Fe_2O_3$/ZnO ternary composite had efficient and selective degradation towards iodoform.

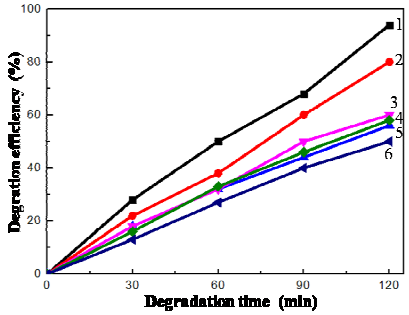


**Fig. 7** Photo-degradation efficiency of iodoform and MO under illumination. The degradation curve of Ag/$Fe_2O_3$/ZnO for iodoform (curve 1), and for MO (curve 2), the degradation curve of $Fe_2O_3$/ZnO for MO (curve 3), and for iodoform (curve 4) , the degradation curve of Ag/ ZnO for iodoform (curve 5), and for MO (curve 6).

### 3.4 The reusability of Ag/$Fe_2O_3$/ZnO composite

To examine the reusability of Ag/$Fe_2O_3$/ZnO ternary composite, it was used as the photocatalysts material for 5 cycles. The iodoform and MO solutions were replaced every 120 min and measured their maximum absorbance, respectively. After every cycle, the corresponding degradation rates of Ag/$Fe_2O_3$/ZnO for iodoform and MO were about 92%, 89%, 86%, 85% and 82%, and 75%, 73%, 71%, 70% and 68% (Fig. 8b), respectively. The degradation efficiency of Ag/$Fe_2O_3$/ZnO ternary composite for iodoform and MO solutions dropped about 10% and 7% after 5 cycles (Fig. 8a), respectively. The reason may be that Ag/$Fe_2O_3$/ZnO ternary composite participates in the process of degradation, there are some consumption of Ag/$Fe_2O_3$/ZnO after every cycle.

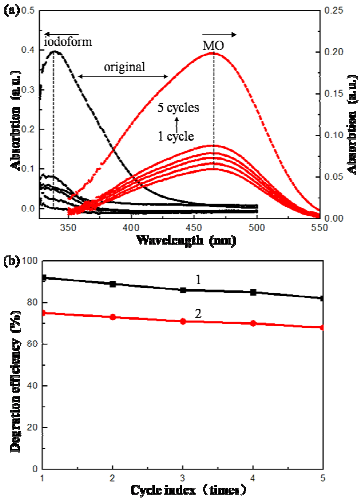

**Fig. 8** (a) Cycle times-dependent absorption spectra of iodoform and MO solutions degraded by Ag/$Fe_2O_3$/ZnO ternary composite, and (b) the cycle degradation curves of Ag/$Fe_2O_3$/ZnO for iodoform (curve 1), and for MO (curve 2).

### 3.5 The proposed mechanism of enhancement of photocatalytical activity by Ag/$Fe_2O_3$/ZnO

The different component between Ag/$Fe_2O_3$/ZnO ternary composite, $Fe_2O_3$/ZnO and Ag/ZnO binary composite may result in the difference on photocatalytic activities. The proposed photocatalytic degradation mechanism of iodoform and MO by Ag/$Fe_2O_3$/ZnO is illustrated in Fig. 9. The process can be described as follows: 1) under illumination, the electrons of ZnO in the Ag/$Fe_2O_3$/ZnO are excited to generate electron-hole pairs, 2) the electrons in the valence band (VB) of ZnO are transferred to (CB) conduction band of $Fe_2O_3$, 3) and then they are transferred to CB of Ag. The high separation rate of electron-hole pairs makes it easier to form $O^{2-}$ active ion and OH· radicals on the surface of Ag/$Fe_2O_3$/ZnO to degrade iodoform and MO, and to enhance the photo-degradation activity, the process can be written as [20-25]:

$$O_2 + e^- \rightarrow O_2^- \quad (1)$$

$$O_2^- + H^+ \rightarrow HO_2\cdot \quad (2)$$

$$2HO_2\cdot \rightarrow H_2O_2 + O_2 \quad (3)$$

$$H_2O_2 + O_2^- \rightarrow OH^\cdot + O_2 + OH^- \quad (4)$$

$$OH^\cdot + \text{pollutants} \rightarrow CO_2 + H_2O \quad (5)$$

At the same time, under the action of $H^+$ and $e^-$, iodoform can be decomposed by Ag due to the following reactions [26-28]:

$$Ag^+ \rightarrow Ag^{2+} + e^- \quad (6)$$

$$Ag^{2+} + H_2O \rightarrow Ag^+ + H^+ + OH^\cdot \quad (7)$$

$$CHI_3 + 3H^+ + 3e^- \rightarrow CH_4 + 3I^- \quad (8)$$

$$CH_4 + OH^\cdot \rightarrow H_2O + CO_2 \quad (9)$$

$$I^- + Ag^+ \rightarrow AgI \quad (10)$$

This provides another way for the Ag/$Fe_2O_3$/ZnO to degrade iodoform, which can improve the degradation efficiency of iodoform. Taken together, the above reactions account for the selective property of Ag/$Fe_2O_3$/ZnO ternary composite towards iodoform degradation [29].

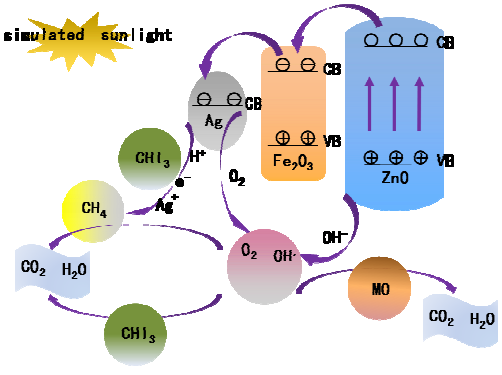


**Fig. 9** The diagrammatic sketch of iodoform and MO degraded by the Ag/$Fe_2O_3$/ZnO ternary composite.

## 4. Conclusions

In summary, the Ag/$Fe_2O_3$/ZnO ternary composite has been successfully synthesized via chemical deposition and photochemical deposition in aqueous solution. The Ag/$Fe_2O_3$/ZnO ternary composite shows a much higher photocatalytic performance compared with $Fe_2O_3$/ZnO or Ag/ZnO binary composite. Moreover, the Ag/$Fe_2O_3$/ZnO ternary composite has efficient and selective degradation of carcinogenic iodoform in the sewage. This provides a promising strategy for efficient degradation of halogenated hydrocarbon.

## Acknowledgements

We acknowledge the financial support from the Ministry of Education of China (IRT1148), the Priority Academic Program Development of Jiangsu Higher Education Institutions (YX03001), the Natural Science Foundation of Jiangsu Province (BK20131376, BY2014015), the Opening Project of State Key Laboratory of New Ceramic and Fine Processing(KF201310) and the Synergistic Innovation Center for Organic Electronics and Information Displays.

## References

1. M. Veldhoen, K. Hirota, A. M. Westendorf, J. Buer, L. Dumoutier, J.-C. Renauld and B. Stockinger, Nature, 2008, 106-109.
2. J. W. Harper, Nature, 2007, 499-500.
3. L. L. Xu, B. Wei, W. L. Liu, H. L. Zhang, C. Y. Su and J. X. Che, Nanoscale Res. Lett, 2013, 536.
4. J. F. Lei, L. B. Li, X. H. Shen, K. Du, J. Ni, C. J. Liu and W. S. Li, Langmuir, 2013, 13975-13981.
5. V. VS and L. BV, Nature, 2015, 41-42.
6. B. Yin, Y. Qiu, H. Q. Zhang, J. X. Lei, Y. Chang, J. Y. Ji, Y. M. Luo, Y. Zhao and L. Z. Hu, RSC Adv, 2015, 11469-11474.
7. M. Lan, G. L. Fan, L. Yang and F. Li, RSC Adv, 2015, 5725-5734.
8. J. J. D. Yoreo, P. U. P. A. Gilbert, N. A. J. M. Sommerdijk, R. L. Penn, S. Whitelam, D. Joester, H.Z. Zhang, J. D. Rimer, A. Navrotsky, J. F. Banfield, A. F. Wallace, F. M. Michel, F. C. Meldrum, H. Cölfen and P. M. Dove, Science, 2015.
9. J. J. Xue, S. S. Ma, Y. M. Zhou, Z. W. Zhang and P. Jiang, RSC Adv, 2015, 18832-18840.
10. H. R. Liu, G. X. Shao, J. F. Zhao, Z. X. Zhang, Y. Zhang, J. Liang, X. G. Liu, H. S. Jia and B. S. Xu, J. Phys. Chem. C, 2012, 16182-16190.
11. C. L. Zhang, M. F. Shao, F. Y. Ning, S. M. Xu, Z. H. Li, M. Wei, D. G. Evans and X. Duan, Nano Energy, 2015, 231-239.
12. L. Zhang, H. Z. Li, Y. Liu, Z. Tian, B. Yang, Z. B. Sun and S. Q. Yan, RSC Adv, 2014, 48703-48711.
13. S. R. Wang, J. X. Zhang, J. D. Yang, X. L. Gao, H. X. Zhang, Y. S. Wang and Z. Y. Zhu, RSC Adv, 2015, 10048-10057.

14. C. Karunakaran, P. Vinayagamoorthy and J. Jayabharathi, Langmuir, 2014, 15031-15039.
15. A. Wei, L. H. Pan and W. Huang, Mater. Sci. Eng. B-Adv, 2011, 1409-1421.
16. Y. J. Liu, L. Sun, J. G. Wu, T. Fang, R. Cai and A. Wei, Mater. Sci. Eng. B-Adv, 2015, 9-13.
17. M. Behrens, F. Studt, I. Kasatkin, S. Kühl, M. Hävecker, F. Abild-Pedersen, S. Zander, F. Girgsdies, P. Kurr, B.-L. Kniep, M. Tovar, R. W. Fischer, J. K. Nørskov and R. Schlögl, Science, 2012, 893-897.
18. T. T. Jiang, X. Y. Qin, Y. Sun and M. Yu, RSC Adv, 2015, 65595-65599.
19. J. N. Schrauben, R. Hayoun, C. N. Valdez, M. Braten, L. Fridley and J. M. Mayer, Science, 2012, 1298-1301.
20. N. T. Khoa, S. W. Kim, D.-H. Yoo, S. Cho, E. J. Kim and S. H. Hahn, ACS Appl. Mater. Inter, 2015, 3524-3531.
21. K. Wu, J. Chen, J. R. McBride and T. Lian, Science, 2015, 632-635.
22. T. G. Xu, L. W. Zhang, H. Y. Cheng and Y. F. Zhu，Appl. Catal. B-Environ, 2011, 382-387.
23. Y. L. Lai, M. Meng and Y. F. Yu, Appl. Catal. B-Environ, 2010, 491-501.
24. X. M. Hou and L. X. Wang, RSC Adv. 2014, 56945-56951.
25. B. X. Li and Y. F. Wang, Superlattice. Microst, 2010, 615.
26. C. Comninellis,Electrochim. Acta, 1994, 1857-1862.
27. S. A. Ansari, M. M. Khan, M. O. Ansari, J. Lee and M. H. Cho, J. Phys. Chem. C, 2013, 27023-27030.
28. C. L. Parworth, M. K. Tucker, B. E. Holmes and G. L. Heard, J. Phys. Chem. A, 2011, 13133-13138.
29. J. Liu, Y. Liu, N. Y. Liu, Y. Z. Han, X. Zhang, H. Huang, Y. Lifshitz, S.-T. Lee, J. Zhong and Z. H. Kang, Science, 2015, 970-974.